Relative importance of geostatistical and transport models in describing heavily tailed breakthrough curves at the Lauswiesen site

Monica Riva [a,*], Alberto Guadagnini [a], Daniel Fernandez-Garcia [b],
Xavier Sanchez-Vila [b], Thomas Ptak [c]

[a] *DIIAR, Politecnico di Milano, Piazza L. Da Vinci 32, 20133 Milano, Italy*
[b] *Department of Geotechnical Engineering and Geosciences, Technical University of Catalonia, Gran Capità S/N, 08034 Barcelona, Spain*
[c] *University of Göttingen, Geosciences Center, Goldschmidtstrasse 3, D-37077 Göttingen, Germany*

ARTICLE INFO

ABSTRACT

We analyze the relative importance of the selection of (1) the geostatistical model depicting the structural heterogeneity of an aquifer, and (2) the basic processes to be included in the conceptual model, to describe the main aspects of solute transport at an experimental site. We focus on the results of a forced-gradient tracer test performed at the "Lauswiesen" experimental site, near Tübingen, Germany. In the experiment, NaBr is injected into a well located 52 m from a pumping well. Multilevel breakthrough curves (BTCs) are measured in the latter. We conceptualize the aquifer as a three-dimensional, doubly stochastic composite medium, where distributions of geomaterials and attributes, e.g., hydraulic conductivity (K) and porosity (ϕ), can be uncertain. Several alternative transport processes are considered: advection, advection–dispersion and/or mass-transfer between mobile and immobile regions. Flow and transport are tackled within a stochastic Monte Carlo framework to describe key features of the experimental BTCs, such as temporal moments, peak time, and pronounced tailing. We find that, regardless the complexity of the conceptual transport model adopted, an adequate description of heterogeneity is crucial for generating alternative equally likely realizations of the system that are consistent with (a) the statistical description of the heterogeneous system, as inferred from the data, and (b) salient features of the depth-averaged breakthrough curve, including preferential paths, slow release of mass particles, and anomalous spreading. While the available geostatistical characterization of heterogeneity can explain most of the integrated behavior of transport (depth-averaged breakthrough curve), not all multilevel BTCs are described with equal success. This suggests that transport models simply based on integrated measurements may not ensure an accurate representation of many of the important features required in three-dimensional transport models.

© 2008 Elsevier B.V. All rights reserved.

1. Introduction

The success of environmental risk assessment and remediation practices of contaminated groundwater bodies strongly relies on the characterization of the spatial variations of key hydrogeologic features of aquifers and proper assessment of relevant transport mechanisms and associated parameters. Incorporating these features in stochastic flow and transport models is then conducive to a representation of the system in terms of (a) relevant (statistical) moments of solute concentrations or, more completely, (b) a set of alternative and equally likely realizations of contaminant distributions. The last 50 years have been characterized by intense and exciting debates which have led to significant advances in theoretical and operational development of stochastic and/or deterministic (numerical/analytical) techniques for the analysis of flow and transport in the subsurface under a variety of conditions. In this context, major issues of concern in hydrogeology include modeling of heterogeneity

---

* Corresponding author.
E-mail address: monica.riva@polimi.it (M. Riva).

of hydrogeologic properties and relevant processes governing solute transport [see the recent compilation of de Marsily et al., 2005].

Tracer tests have traditionally been regarded as appropriate and efficient tools to infer information about aquifer properties at various scales of interest (laboratory and field scales) and for various flow regimes (natural or forced-gradient conditions). For a review of modern tracer testing techniques, the interested reader is referred to the work of Ptak et al. (2004).

Interpretation of tracer tests performed in real sites faces many challenges. On one hand, it is important to properly choose the underlying transport equation amongst a set of models ranging from the classical ADE (advection–dispersion equation) to CTRW (continuous time random walk). A recent review of drawbacks and merits of various techniques for the reproduction of observed tracer plumes, as reflected by BTCs (breakthrough curves) or spatial distributions of concentrations, is offered by Berkowitz et al. (2006). Second, due to our incomplete knowledge of the system, which is persistent at all scales of investigation, one should be very careful when using a deterministic approach to interpret observed BTCs. For example, by disregarding the underlying heterogeneity of the system one might obtain interpreted parameters that are apparently not realistic, but actually contain information about the unsampled heterogeneity (Sanchez-Vila and Carrera, 1997; Fernandez-Garcia et al., 2002). A third challenge comes from the fact that most of the stochastic hydrogeology literature relies on the assumption that spatial variation in hydraulic conductivity is the salient controlling factor that should be included in transport models. The variability of other parameters, such as porosity, as well as the impact of cross-correlation between hydraulic parameters is usually disregarded in real applications, despite it has been shown in synthetic aquifers to produce a significant effect in mass fluxes (Hassan, 2001).

In this context, a salient question is whether the key goal in the interpretation of a given tracer test is to obtain the best possible fit to the measurements by means of models that include some representative (flow and transport) parameters, or to explicitly include some measurement of uncertainty associated with modeling results. Here, we look at the problem form the perspective that it is possible to describe the main features of an observed BTC by means of multiple, equally likely manifestations of the system, along the lines of Salamon et al. (2007). Thus, our interest is not to calibrate model parameters but, instead, to evaluate the predictive capability of forward stochastic transport models based on a high-resolution three-dimensional geostatistical description of the test site and on simple conceptual transport models. We illustrate the problem starting from the measurements taken during a tracer test performed at the "Lauswiesen" experimental site (Germany), where four multilevel breakthrough curves were measured within the pumping well, using a flow separation technique. Our distinctive aim is to analyze the importance of properly modeling the uncertain distribution of geomaterials and associated attributes (hydraulic conductivity and porosity) on our ability to reproduce the key features of the depth-averaged and multilevel breakthrough curves. These include the first temporal moments and the recorded pronounced tailing.

To this end, we compare the relative impact of (a) the choice of the underlying governing transport processes (i.e., advection, dispersion — either local or macroscale − and/or mass-transfer between mobile and immobile matrix phases) and (b) the choice of different models to describe the (random) heterogenity of the system (i.e., only hydraulic conductivity or both conductivity and porosity display random variations) on our ability to reproduce the observed features of the BTCs. In this context, we perform numerical flow and transport simulations within a Monte Carlo framework upon treating the aquifer as a three-dimensional, doubly stochastic composite medium.

The structure of the paper is as follows. We devote Section 2 to a brief description of the experimental field site and the outline of the aquifer characterization procedures and tracer test design and implementation. Then, we present the details of the numerical modeling technique in Section 3. Section 4 compares the features of the (probabilistic) BTCs obtained upon incorporating in our procedure different conceptual models of the heterogeneous structure of the site. Finally, we summarize the main results and conclusions of this paper.

2. Field setting and experiments

The aquifer under investigation is located at the "Lauswiesen" experimental field site (Fig. 1), near Tübingen in the Neckar river valley. An extensive presentation of the main geological features and hydrogeologic characterization of the site has been offered by Riva et al. (2006). For the sake of completeness, here we briefly summarize the field setting and aquifer characterization results. Then we present details of the tracer test.

2.1. Outline of field setting and characterization

The aquifer consists of alluvial material overlain by stiff silty clay and underlain by hard silty clay. The lithostratigraphic characterization has been performed on the basis of the stratigraphy obtained from the drilling of 150 mm-diameter monitoring wells (Sack-Kühner, 1996; Martac and Ptak, 2003) and of one 400 mm-diameter pumping well. The location of monitoring and pumping wells is shown in Fig. 1. The wells were drilled until the marly bedrock constituting the impermeable aquifer bottom of variable depth was identified. The aquifer saturated thickness is about 5 m. Water table measurements showed a regional hydraulic gradient of about 0.1–0.2% with a general groundwater flow direction from South-West toward North-East. As detailed by Riva et al. (2006), general groundwater flow and transport patterns in the area have been analyzed by means of an existing deterministic two-dimensional model, covering an area of about 3×1 km^2 which includes the test site. On these bases, average porosity $\phi = 9.8\%$ was obtained by fitting individually simulated breakthrough curves to those obtained from depth-averaging of multilevel–multitracer field experiments.

Extensive field and laboratory scale aquifer investigation procedures, including sieve analyses, flowmeter measurements and pumping tests were applied. The sieve analyses, performed on drill core samples (taken as point measurements, compared to the scale of the investigation domain)
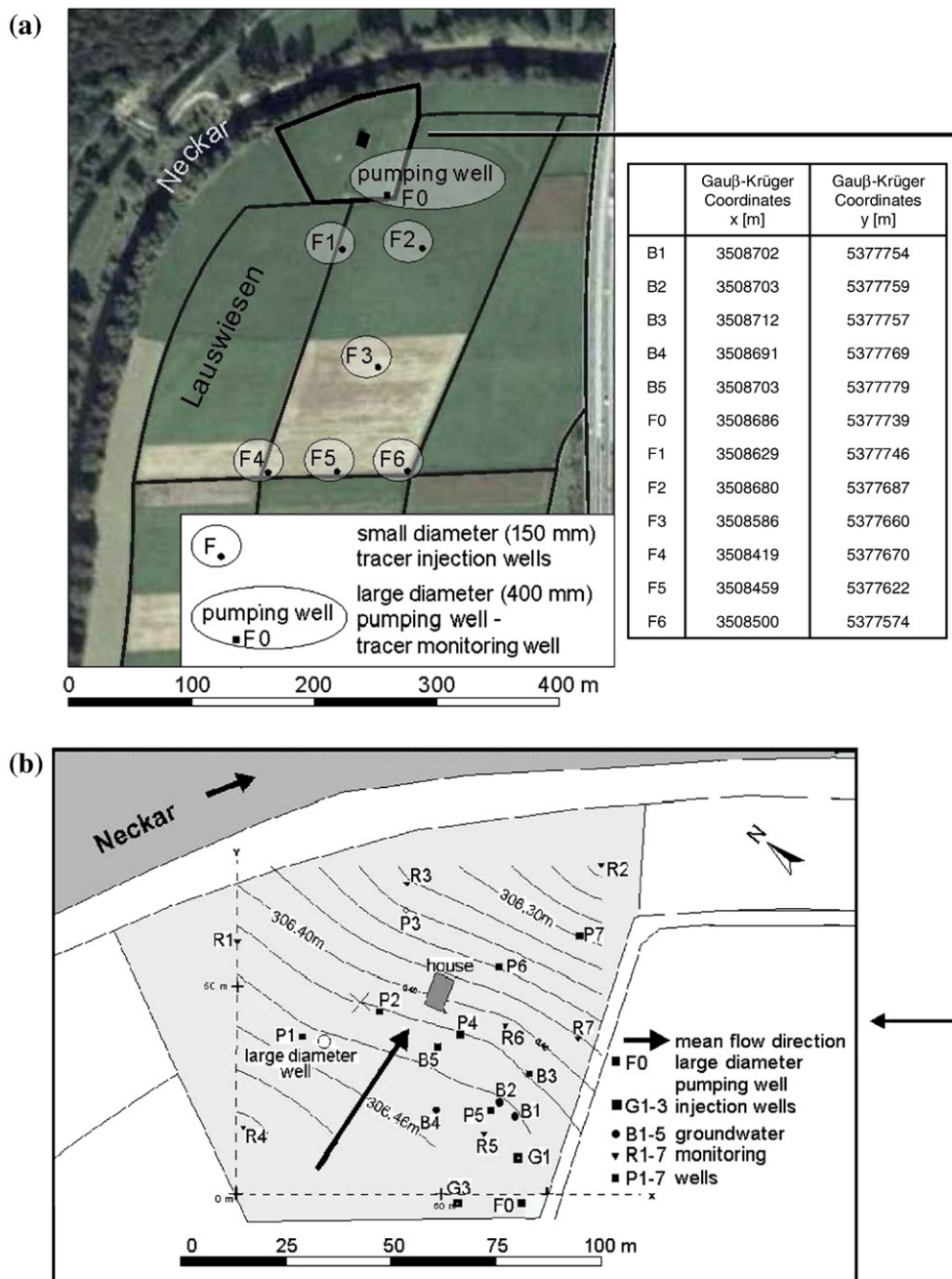
	Gauβ-Krüger Coordinates x [m]	Gauβ-Krüger Coordinates y [m]
B1	3508702	5377754
B2	3508703	5377759
B3	3508712	5377757
B4	3508691	5377769
B5	3508703	5377779
F0	3508686	5377739
F1	3508629	5377746
F2	3508680	5377687
F3	3508586	5377660
F4	3508419	5377670
F5	3508459	5377622
F6	3508500	5377574

Fig. 1. Map of the site and location of the pumping and monitoring wells at the "Lauswiesen" site (background from Google Earth). The global piezometric surface based on groundwater level measurements is also reported, together with the estimated general flow direction at the site. From Riva et al. (2006).

indicated very heterogeneous, highly conducive alluvial deposits. More than 400 grain distribution curves are available within the test area. These are distributed along 12 verticals (wells B1, B2, …, B5 and F0, F1, F2, …, F6 in Fig. 1).

A multivariate geostatistical facies-based parameterization approach was applied to characterize the heterogeneous three-dimensional aquifer structure. The analysis comprises three parts: multivariate cluster analysis (MCA), univariate statistics of K, and variography. The complete analysis can be found in Riva et al. (2006), and a short summary is presented here. From the MCA procedure (McQueen, 1967), three different types of aquifer materials (clusters/facies) were identified to describe the heterogeneity of the aquifer lithology. Distributions of K values within each facies were determined from the grain size distribution curves (the results are compiled in Table 1). It is noted that ignoring the existence of different lithologies and treating all samples together leads to a variance of ln K close to 3.0.

Table 1
Main results of the multivariate cluster analysis procedure (K_G and σ_Y^2 respectively are the geometric mean of hydraulic conductivities and variance of natural log-conductivities of samples)

	Cluster 1	Cluster 2	Cluster 3	All samples
Description	Moderately sorted gravel, very few fines and around 13% sand	Poorly sorted gravel, few fines and around 24% sand	Well sorted sand, very few fines and 23% gravel	
Percentage of samples	53	44	3	100
K_G [m/s]	5.92×10^{-3}	0.83×10^{-3}	0.31×10^{-3}	2.22×10^{-3}
σ_Y^2	2.41	1.35	0.32	2.97

Table 2
Main results of the three-dimensional geostatistical analysis of $Y = \ln K$

	Cluster 1	Cluster 2	All samples
Variogram type	Spherical	Spherical	Spherical
Nugget	0.05	0.05	0.05
Sill	2.36	1.30	2.86
Horizontal range [m]	10	10	12
Vertical range [m]	0.90	0.80	0.90

Results are presented separately for samples of cluster 1 and cluster 2 and by analyzing jointly all samples collected in the system as if they belonged to a single, homogenized, lithofacies.

Finally, the variography analysis was divided in two successive steps. First, indicator variography is used to characterize the spatial distribution of facies. All indicator variograms display a slight horizontal anisotropy, with largest horizontal ranges between 11 m (for Clusters 1 and 2) and 35 m (for Cluster 3) and a smallest range of about 6 m for all clusters. Vertical ranges are of the order of 0.5 m. The next step was obtaining the variograms for the $Y = \ln K$ values. The analysis was performed separately for clusters 1 and 2 (cluster 3 values were taken as constant since its relative volumetric fraction is only 3% and the corresponding internal variability of Y is relatively modest, as illustrated in Table 1) and upon considering all samples jointly (all belonging to a single Spatial Random Function). All Y random functions can be modeled by means of axisymmetric variograms, with a vertical range significantly smaller than its horizontal counterpart. Table 2 summarizes the main parameters of the variogram models.

Following Riva et al. (2006), we adopt an experimentally derived linear relationship between the (natural) logarithms of effective porosity and hydraulic conductivity. We note that joint measurements of porosity, ϕ, and hydraulic conductivity were not available at the Lauswiesen site. Thus the relationship between ϕ and K was derived on the basis of data collected at a nearby site (Horkheimer Insel site, as reported by Ptak and Teutsch, 1994) where hydraulic conductivity was obtained from permeameter measurements using 100 mm diameter drill core samples of the Neckar valley aquifer and sieve analyses, while ϕ was evaluated from gravity drainage after the permeameter measurements. The mean drainage porosity ranges between 1.1% and 18.6% with an arithmetic mean equal to 9.3%. On the bases of the information presented by Ptak and Teutsch (1994), the following empirical relationship was assumed (when K is expressed in m/s):

$$\ln \phi = a \ln K + b; \qquad a = 0.350; \quad b = -0.186 \qquad (1)$$

2.2. Column tracer tests

During the drilling of the wells at the "Lauswiesen" site, plastic liners were used to collect continuous aquifer material core samples. A laboratory tracer experiment was performed using a 0.50 m long, 0.10 m diameter, column filled with aquifer material. Small flow rate (4×10^{-6} m³/min) peristaltic pumps were used to induce an effective transport velocity comparable to field conditions. A slug injection of sodium-bromide was performed and electrical conductivity measure-

ments were taken at the column outlet. The resulting breakthrough curve was interpreted by means of the analytical solution of Sauty (1980), which is based on an ADE approach. This provided an estimated dispersivity value, $\alpha \cong 0.08$ m, and a porosity estimate of about 13%. The good fitting between the data and the interpretation with the ADE model is reproduced in Fig. 2.

2.3. Forced-gradient field tracer tests

To investigate solute transport behavior at the field scale in three dimensions, a multilevel–multitracer technique was developed and tested at the site (Ptak et al., 2004). The tracer testing was run under Dirac type tracer injection and convergent flow forced-gradient conditions. A complete description of the instrumentation, injection and sampling technique is presented by Martac and Ptak (2003) and Ptak et al. (2004).

Here, we focus on the convergent flow field test where groundwater was pumped out of well F0 using a suction pump (pumped flow rate $Q = 14$ l/s), and the tracer was injected instantaneously into well F2 (located at a distance of 52 m from F0; see Fig. 1), and four multilevel breakthrough curves were measured within the pumping well itself using a flow separation technique (Ptak et al., 2004). A depth-
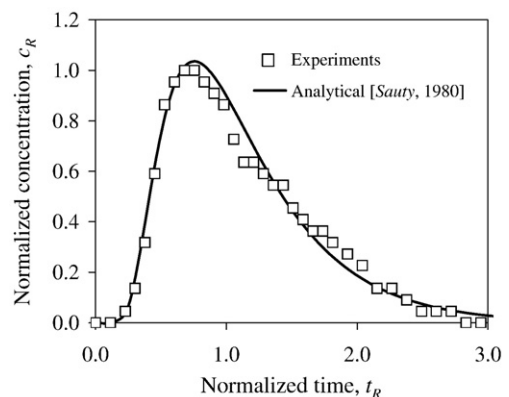

Fig. 2. Results of the calibration procedure for the laboratory scale tracer experiment. Normalized concentration, $c_R = c/c_{max}$, where c is concentration and c_{max} is the maximum observed concentration. Normalized time, $t_R = (q\,t)/(\phi\,L)$, where q is Darcy's flux, ϕ is porosity, t is time, and L is the length of the column. Data are properly fitted by means of an ADE with two fitting parameters (dispersivity and porosity).

averaged BTC was then obtained on the basis of the recorded multilevel BTCs, according to:

$$c_{int}(t) = \sum_{j=1}^{n} f_j c_j(t) \qquad (2)$$

Here, $c_{int}(t)$ is the depth-averaged concentration at time t, $n = 4$ is the number of multilevel BTCs recorded, $c_j(t)$ is the concentration measured at level j and time t. The thickness associated with each individual concentration sampling level, Δz_j ($j = 1, 2, 3, 4$) is (levels are numbered in ascending order from the bottom, i.e., level 1, to the top, i.e., level 4, of well F0): $\Delta z_1 = \Delta z_2 = \Delta z_3 = 0.75$ m, $\Delta z_4 = 1.35$ m.

The volumetric flux fraction associated with level j, f_j, can be calculated on the basis of the available impeller flowmeter measurements at well F0, as:

$$f_j = \frac{\sum_{i=1}^{N_j} (K_i \cdot \Delta z_i)}{\sum_{i=1}^{N} (K_i \cdot \Delta z_i)} \qquad (3)$$

Here, N_j and N respectively are the number of vertical intervals with flowmeter records included in level j and the total number of vertical intervals at well F0, and K_i is the hydraulic conductivity representative of a vertical interval of thickness Δz_i. The measured conductivities correspond to vertical intervals ranging in length from 3 to 35 cm. Details of the impeller flowmeter location are presented in Martac and Ptak (2003), where it can be seen that the vertical description of K from direct flowmeter measurements in F0 is available only for the upper part of the well (approximately 1.36 m from the mean groundwater level). In absence of additional information, we set hydraulic conductivity as uniformly distributed along the remaining part of the borehole and fixed its value as the weighted average of the conductivities measured in the upper part of the well. The volumetric flow fractions associated with each concentration sampling level and calculated on the basis of (3) are: $f_1 = f_2 = f_3 = 0.19$, and $f_4 = 0.43$.

After a quasi-steady-state flow regime was reached, sodium-bromide was injected at F2 (injection time was 80 s, and injected mass was 15 kg). To create a pulse-like injection condition, the injection well was immediately flushed with groundwater to force the tracer into the aquifer. Continuous re-mixing in the injection well was carried out by pumping water from the bottom of the well, and re-injecting it close to the surface. This operation was performed for 48 h. Bromide concentrations were obtained by ion chromatography.

Fig. 3 depicts the four multilevel breakthrough curves recorded at well F0 together with the depth-integrated BTC obtained by Eqs. (2) and (3).

The total mass recovered in F0 after 21 days from injection is about 40% of the injected mass. This is possibly caused by a combination of a number of factors: mass trapped at the bottom of the injection well driven by density contrasts, development of imperfect convergent conditions (transient behaviour of the groundwater flow field), local-scale heterogeneities around the injection and pumping wells (in particular possible small-scale low conductivity zones between the well construction and surrounding media, i.e. skin), and limitation of the total BTC observation time.
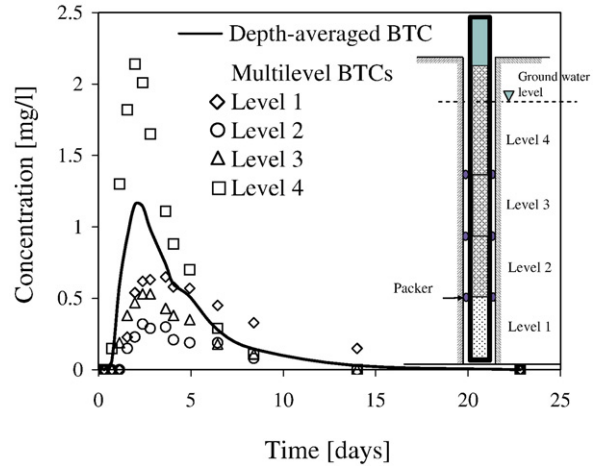

Fig. 3. Recorded multilevel BTCs at pumping well F0 and resulting depth-averaged BTC obtained from Eqs. (2) and (3).

The analysis of the individual multilevel BTCs indicates that mass recovery at the pumping well is not uniformly distributed along the vertical. Specifically, more than the 80% of the mass recovery occurs at levels 1 (21% of total recovery) and 4 (62%). Mass recovery at levels 2 and 3 is about 7% and 10%, respectively, probably indicating that these two levels are representative of some low-conducive flow paths within the system. All the curves are characterized by heavy tails, thus pointing at the existence of anomalous (non-Fickian) transport behavior at the site.

3. Modeling approach

For the numerical modeling, we concentrate on the region of size of about 800 m × 800 m × 8 m, including wells F0 and F2, within which Riva et al. (2006) have developed a stochastic three-dimensional flow model (see Fig. 4). The stochastic variability of geomaterials and their attributes is modeled within the rectangular region (of size 250 m × 400 m × 8 m) reported in Fig. 4, while the remaining part of the aquifer is considered as a homogeneous system. A three-dimensional block-centered finite different grid comprising a total of 2.90×10^6 cells was used. Refinement of cell sizes was performed in the proximity of wells (where cells sizes were set to 0.33 m × 0.40 m × 0.30 m) with gradual increasing of cells sides with distance. The boundary conditions and additional information can be found in Riva et al. (2006).

Amongst various different possibilities, we conceptualize the heterogeneous aquifer as a doubly stochastic process. First, the spatial distribution of the different material blocks is random; second, the distribution of attributes (hydraulic conductivity and porosity) within each identified material block is also random. The lithofacies distribution is described via the indicator geostatistical analysis and hydraulic conductivity is modeled as a correlated random process within each material. Attributes of different materials are considered uncorrelated (Winter et al., 2003). Two models of heterogeneity are considered: (1) HM1: porosity is kept constant throughout the domain; (2) HM2: the distribution of porosity
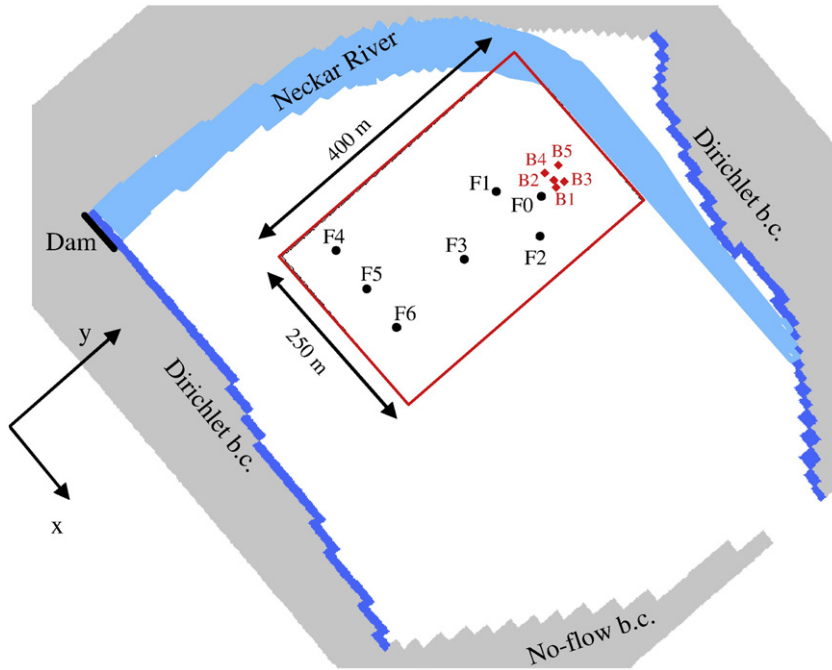
Fig. 4. Limits of the local three-dimensional model. The rectangular region highlighted demarcates the sub-domain within which the aquifer is modeled as a doubly stochastic process. In the remaining of the domain parameters were taken as homogeneous. From Riva et al. (2006).

is linked to the spatial variability of hydraulic conductivity according to the linear relationship described in Section 2.1.

One hundred Monte Carlo iterations were performed for each of the heterogeneous models considered. The sequential indicator simulator of categorical variables SISIMPDF (Deutsch and Journel, 1998) was used to obtain multiple conditional three-dimensional spatial distributions of the three identified facies, with blocks of size 2.0 m × 1.0 m × 0.3 m. When finer discretization is required for computational purposes, each block is then further divided into smaller cells with the same value of hydraulic conductivity. When a well falls within a cell, the subdivision into smaller cells is performed by assigning a higher conductivity to the cell containing the well (K=2.0 m/s) while a smaller value (K=0.2 m/s) is assigned to the cells located around the well to simulate the presence of a gravel pack [e.g., Juhasz, 2001].

The random distribution of conductivity considered was simulated according to the following steps: (a) three-dimensional unconditional realizations of log-conductivities of Clusters 1 and 2 were generated on the same grid by using the code GCOSIM3D (Gómez-Hernández and Journel, 1993); hydraulic conductivity of *Cluster 3* was taken as constant and equal to its geometric mean (this modeling choice is justified by the observation that the relative volume occupied by this type of material is low and the corresponding internal variability of log-hydraulic conductivity is relatively modest, σ_Y^2=0.32); (b) appropriate conductivity values were then assigned to the numerical blocks according to the indicator distribution.

Simulations of the steady-state flow problem for each Monte Carlo realization were conducted with the finite difference code MODFLOW2000 (Harbaugh et al., 2000). Constant pumping (Q=0.014 m³/s) at the (fully screened) well

F0 was simulated by a concentrated sink at the bottom of the aquifer at the planar location identified by F0.

Various conceptual models of transport, differing in terms of the governing basic processes included, are investigated for each Monte Carlo iteration: (a) purely advective transport; (b) an advection–dispersion model (ADE); and (c) a double porosity model, with mass-transfer between mobile and immobile regions. The latter is described by the following governing equations (Haggerty et al., 2001):

$$\phi_m \frac{\partial c_m}{\partial t} + \phi_{im} \frac{\partial c_{im}}{\partial t} = -q\nabla c_m + \nabla \cdot (\phi_m \mathbf{D} \nabla c_m) \tag{4}$$

$$\frac{\partial c_{im}}{\partial t} = \beta(c_m - c_{im}) \tag{5}$$

with appropriate initial and boundary conditions. Here, ϕ_m and ϕ_{im} are the porosities of the mobile and immobile regions, respectively associated with solute concentrations c_m and c_{im}; β [T⁻¹] is the effective mass-transfer coefficient; q is the Darcy velocity; and $\mathbf{D}$ is the hydrodynamic dispersion tensor. We emphasize that mass-transfer processes are used to represent subgrid Darcy-scale mass fluxes which are not explicitly described by the numerical flow model. Thus, the immobile domain essentially depicts subgrid low velocity areas where solute mass can enter and temporarily be delayed with respect to processes occurring within mobile regions. In our application, the effect of local-scale dispersion was assumed to be negligible as compared to the mass-transfer processes caused by subgrid heterogeneity.

Tracer transport was simulated with the random walk particle tracking code RW3D (Fernandez-Garcia et al., 2005; Salamon et al., 2006). The approach is computationally efficient and not affected by problems associated with

numerical dispersion (Salamon et al., 2007). The random walk code uses a hybrid scheme for the velocity interpolation that provides local as well as global divergence-free velocity fields within the solution domain. It also provides a continuous dispersion tensor field that approximates well mass balance at grid interfaces of adjacent cells with contrasting hydraulic conductivities (LaBolle et al., 1996; Salamon et al., 2006). A constant-displacement scheme (Wen and Gómez-Hernández, 1996), which modifies automatically the time step size for each particle according to the local velocity is employed in order to decrease computational effort. Mass-transfer processes are efficiently incorporated by switching the state of the particle between mobile/immobile matrix phases according to appropriate transition probabilities (Salamon et al., 2006).

When modeling transport on the basis of the ADE, a local-scale (Darcy scale) longitudinal dispersivity was fixed at 0.10 m, close to the value obtained from the laboratory tracer test results described in Section 2.2. For the purpose of our simulations, transverse horizontal and vertical local-scale dispersivity values were chosen to be one order of magnitude less than the longitudinal dispersivity, resulting in a value of 0.01 m.

In the double porosity model we set $\phi_{im}=0.6\ \phi$ and $\phi_m=0.4\ \phi$. These values have been adopted according to the results of a sensitivity analysis (performed for a limited set of Monte Carlo simulations) on the value of ϕ_{im} and the ratio ϕ_{im}/ϕ_m. In a first set of analyses (sensitivity scenario A), the mobile porosity, ϕ_m, was considered as a random variable linked to K by Eq. (1). Three cases were analyzed for ϕ_{im}: (i) $\phi_{im}=2\%$; (ii) $\phi_{im}=10\%$ and (iii) $\phi_{im}=\phi_m$. We note that the spatial distribution of the total porosity in these three cases is not constant. We then evaluated the effect of changes in ϕ_{im} and ϕ_m in three cases (sensitivity scenario B): (i) $\phi_m=0.5\phi$, $\phi_{im}=6\%$; (ii) $\phi_m=\phi_{im}=0.5\phi$; and (iii) $\phi_m=0.4\phi$, $\phi_{im}=0.6\phi$. Here ϕ is the porosity obtained by Eq. (1). These preliminary results highlighted that: (a) the concentration values obtained in the sensitivity scenario B provide a better representation of the rising limb of the experimental (depth-averaged) BTC curve and of the time at which the concentration reaches its peak (this suggests that the porosity obtained with Eq. (1) can be better interpreted as some representative value of the total amount of mobile and immobile porosity rather than strictly an effective one); (b) the results obtained with ($\phi_m=\phi_{im}=0.5\phi$) and with ($\phi_m=0.4\phi$, $\phi_{im}=0.6\phi$) are very similar. This suggests that one would have a really hard time discriminating between the results obtained using these two different sets of parameters in a stochastic framework.

Tracer injection in the model was performed upon uniformly allocating 20,000 particles, each having the same normalized mass fraction, along the vertical corresponding to the location of well F2 and releasing them instantaneously. The normalized injected mass was calculated on the basis of the mass recovered during the test. A sensitivity analysis performed for a few Monte Carlo iterations on the number of particles revealed that 20,000 particles result in a good compromise between the computational time and the accuracy of the reconstructed multilevel BTCs.

The assessment of the ability of a given model to reproduce (in an ensemble sense) the key features of contaminant transport during the tracer test was performed upon analyzing the following different quantities, associated with the measured and modeled (integrated and multilevel) BTCs:

(1) the non-centered first order moment, T_1, linked to the mean advective time of the system; it is defined as

$$T_1 = \frac{\int_0^\infty tc(t)dt}{\int_0^\infty c(t)dt} \qquad (6)$$

where, $c(t)$ is the concentration (measured or computed) at the observation well at time t (in the double porosity model, $c(t)$ it is the mobile concentration);
(2) the centered second order moment, τ_2, defined as

$$\tau_2 = \frac{\int_0^\infty [t-T_1]^2 c(t)dt}{\int_0^\infty c(t)dt} \qquad (7)$$

which provides a measure of the spreading the BTC around its center of mass; (3) the skewness coefficient, C_s, rendering a measure of the symmetry of the BTC, and defined as

$$C_s = \frac{\int_0^\infty [t-T_1]^3 c(t)dt}{\left[\int_0^\infty [t-T_1]^2 c(t)dt\right]^{3/2}} \left[\int_0^\infty c(t)dt\right]^{1/2} \qquad (8)$$

(4) the peak concentration, c_{peak}, the time at which c_{peak} is attained, t_{peak}, and the time of first arrival of solute, t_a;
(5) the slope of the tail of the BTC in semilog plot.

The above quantities are calculated for each BTC obtained within the Monte Carlo process and their distributions are compared with the corresponding quantities calculated on the basis of the experimental BTCs. Analysis of convergence of the Monte Carlo simulations evidenced that, even though 100 Monte Carlo iterations do not completely lead to statistical stability, the obtained results allow a meaningful qualitative analysis of the process. A detailed analysis of the results is reported in Section 4.

4. Modeling results and discussion

4.1. Integrated (depth-averaged) breakthrough curve

The impact of accounting for the spatial variability of porosity is analyzed in Fig. 5 when transport is modeled as a purely advective process within each Monte Carlo iteration. Fig. 5a,b contrast the integrated experimental BTC against the ensemble average and median BTCs obtained for the geostatistical heterogeneity model HM1, respectively with constant porosity $\phi=9.8\%$ (see Section 2.1) and $\phi=13\%$ (see Section 2.2). As seen in Section 2, both values are based on the model of Sauty (1980); while the former value is the average effective porosity obtained by fitting individually each of the multilevel–multitracer field experiments, the latter was derived on the basis of a laboratory scale tracer test.

The experimental BTC is reported in terms of a normalized concentration, $c_{int}^{norm}(t)$ [s^{-1}], defined as

$$c_{int}^{norm}(t) = \frac{Q \cdot c_{int}(t)}{m_0} \qquad (9)$$

where Q [m^3/s] and m_0 [kg] respectively are the total pumping rate at the well and the total mass recovered during the test.
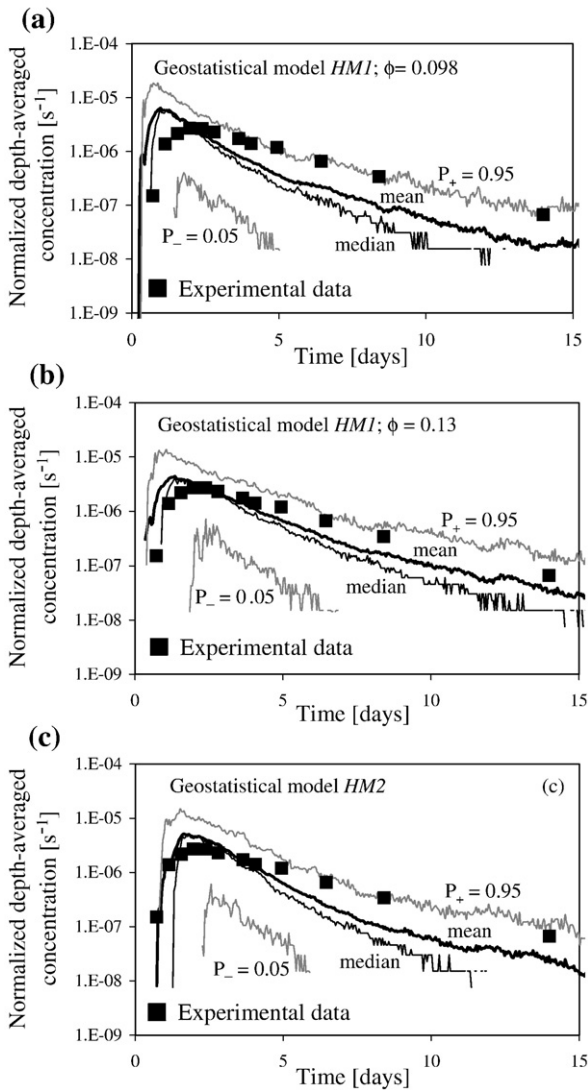
Fig. 5. Depth-averaged (integrated) normalized experimental BTC and ensemble mean and median Monte Carlo-based BTCs for purely advective solute transport: (a) geostatistical model HM1 with constant porosity ϕ=9.8%; (b) geostatistical model HM1 with constant porosity ϕ=13%; and (c) geostatistical model HM2. Monte Carlo-based envelopes associated with probability levels P_+=0.95 and P_-=0.05 are also reported.

Numerical BTCs are also offered in terms of a consistently normalized concentration. Envelopes associated with probability levels P_+=0.95 and P_-=0.05 are also reported in the figure, in order to provide a comprehensive depiction of the range of variability of the Monte Carlo-based BTCs. Fig. 5c, provides the corresponding curves for the geostatistical model HM2. We emphasize that a Monte Carlo procedure offers an ensemble of equally likely realizations of the system and its response to the induced stress (i.e., the tracer injection), and that the observed data are conceptualized as one of an infinite number of alternative possibilities. This is precisely the type of result which is needed in the context of assessment of uncertainty associated with predictions of the system state. As already stated, our aim is not to reconstruct

reality by calibrating flow and transport processes, but to explore the extent at which relevant transport features observed in the field can be consistently reproduced (in an ensemble sense) by different conceptual models, based on a high-resolution three-dimensional geostatistical description of the site.

We note that for all three cases the experimental data lie (with few exceptions) within the bandwidth associated with probability $\Delta P = P_+ - P_- = 0.90$. Adopting a constant porosity leads to a consistent underestimate (in the mean) of the first arrival and peak times. These quantities are better reproduced (in a mean sense) by explicitly incorporating in the procedure the variability of porosity at the site. The pronounced tailing observed in the field is qualitatively captured by the Monte Carlo realizations for all three cases, albeit with different degrees of success. Another interesting result is that inclusion of porosity variability does not dramatically impact the uncertainty associated with predicted BTCs, as qualitatively observed in the figures. These results evidence that, even though heterogeneity of porosity is usually not as pronounced as that of hydraulic conductivity, the description of transport processes at the site greatly benefits from including spatial variability of porosity in the modeling effort.

We then analyze the effect of the different transport processes investigated in the context of the heterogeneity model HM2. Fig. 6a contrasts the integrated (normalized) experimental BTC against the ensemble average and median (normalized) BTCs obtained when transport is depicted by means of a purely advective scheme. Results associated with the complete Monte Carlo set of simulations are also reported in the figure, in order to provide a comprehensive depiction of the range of variability of the Monte Carlo-based BTCs.

A similar depiction is reported in Fig. 6b and c when transport is respectively described by means of an ADE or with a double porosity model, with the fixed (non-calibrated) parameters described in Section 3. In the latter we adopted a spatially uniform mass-transfer rate coefficient, β [T^{-1}]. A sensitivity analysis of the shape of the integrated BTC on β was performed for a limited set of Monte Carlo iterations upon varying β between 10^{-6} and 10^{-4} s^{-1} (indicating a characteristic mass-transfer time from tens to fractions of days, respectively). For each individual realization, the lowest values of β resulted in an early time behavior which is very similar to the response of the system when transport is modeled only by advection. The largest value of β allowed a satisfactory qualitative reproduction of the overall behavior of the measured BTC for each tested Monte Carlo iteration. On these bases, we adopted a constant $\beta = 10^{-4}$ s^{-1} in all simulations presented in this paper.

Fig. 6 reveals that when porosity variability is explicitly included in the structural model of the porous medium, the three transport models considered render quite similar descriptions of the integrated BTC at the site. A relevant feature which can be observed is that the pronounced tailing evidenced by the measurements can be qualitatively reproduced by each of the transport models investigated, albeit with different degree of success, even without resorting to fine calibration of the transport parameters (e.g., by means of stochastic inverse modeling). This is illustrated in Fig. 7, which visually compares the quality of selected simulated breakthrough curves that provide a good qualitative agreement
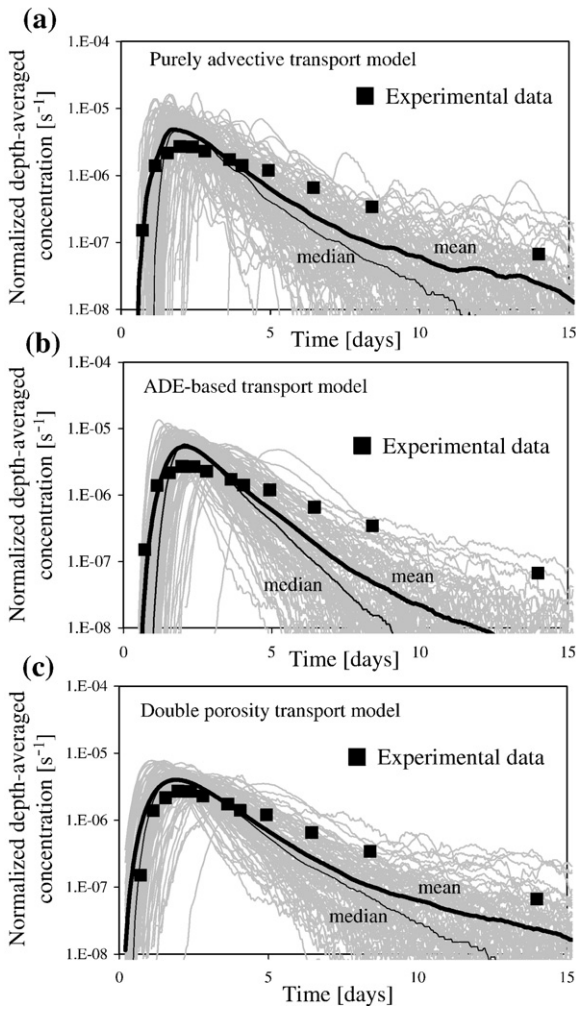
Fig. 6. Depth-averaged (integrated) normalized experimental BTC and ensemble mean and median Monte Carlo-based BTCs for geostatistical heterogeneity model HM2 when transport is depicted by means of (a) purely advective process, (b) an ADE and (c) a double porosity model. Results associated with the complete Monte Carlo set of simulations are also reported.

The following features can be highlighted:

(a) In general, differences amongst the results obtained on the basis of the three transport models tested are mild;

(b) The main statistics of T_1 and τ_2 are similar for the purely advective and the double porosity models and are consistent with the observed reality;

(c) The main statistics and the cumulative distributions of t_{peak}, are similar for the three transport models analyzed and are consistent with available observations;

(d) The model rendering the highest consistency with measurements in terms of the best fit to the c_{peak} and t_a values is the double porosity model;

(e) The ADE model with non-calibrated local-scale dispersivities provides the worst results (in an ensemble sense) for τ_2.
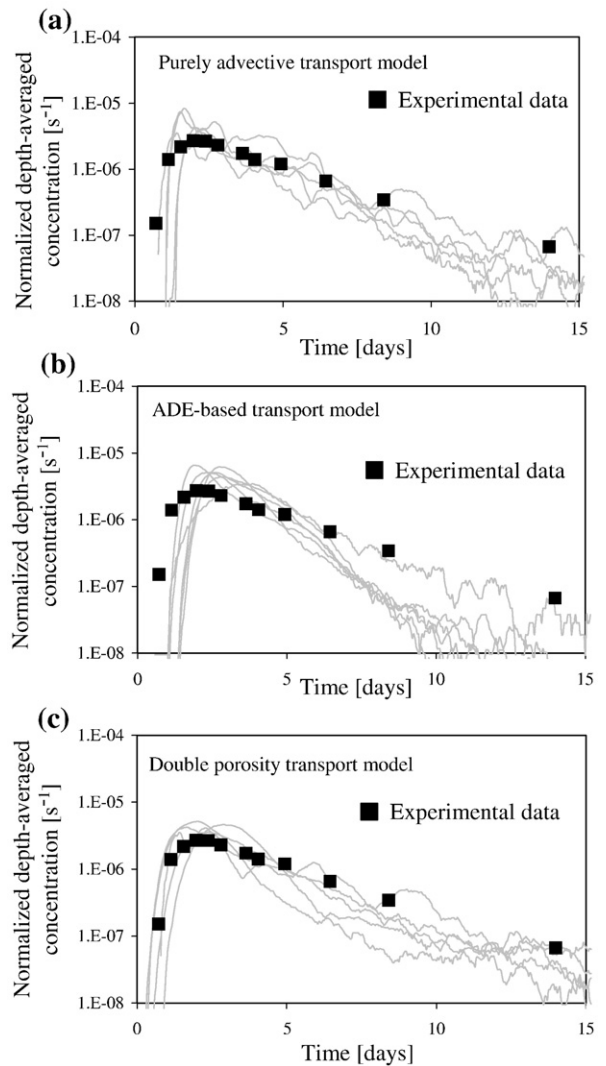

Fig. 7. Depth-averaged (integrated) normalized experimental BTC versus selected Monte Carlo simulations for geostatistical heterogeneity model HM2 when transport is depicted by means of (a) purely advective process, (b) an ADE and (c) a double porosity model.

with the experimental data for the different conceptual transport models adopted.

A quantitative analysis of the results provided by the three transport models examined within the context of the geostatistical model HM2 is presented in Table 3. For each model we report the first three temporal moments, the peak concentration, c_{peak}, the time at which c_{peak} is attained, t_{peak}, and the time of first arrival of solute, t_a, as computed on the basis of the experimental integrated BTC together with the main statistics of the results obtained from our Monte Carlo simulations. Specifically, for each quantity we report the minimum and maximum values, the mean, median and standard deviation, and the values associated with probabilities 0.05, and 0.95. Figs. 8 and 9 depict cumulative distributions of quantities reported in Table 3 as obtained on the basis of numerical Monte Carlo iterations for the three transport models analyzed.

Table 3

Significant statistics of the Monte Carlo-based depth-averaged breakthrough curves for the geostatistical heterogeneity model HM2 and the various transport models analyzed

		T_1 [d]	τ_2 [d^2]	C_S [–]	c_{peak} [s^{-1}]	t_{peak} [d]	t_a [d]
	Experiments	4.378	8.648	1.52	2.71E−6	1.969	0.719
Minimum	Purely advective model	1.554	0.485	0.79	4.16E−6	0.813	0.729
	ADE model	1.473	0.240	0.96	2.77E−6	1.104	0.688
	Double porosity model	1.542	0.678	0.89	2.69E−6	0.854	0.313
Maximum	Purely advective model	9.177	173.750	26.37	3.24E−5	5.021	3.771
	ADE model	5.777	11.886	5.49	1.60E−5	5.063	3.188
	Double porosity model	9.157	173.430	19.22	9.29E−6	5.104	2.188
Mean	Purely advective model	3.328	8.658	4.38	1.14E−5	2.143	1.375
	ADE model	2.928	1.713	2.31	7.67E−6	2.268	1.161
	Double porosity model	3.313	9.005	3.94	5.33E−6	2.190	0.663
Median ($P=0.5$)	Purely advective model	3.090	2.767	3.65	9.92E−6	1.979	1.292
	ADE model	2.788	1.162	2.15	7.49E−6	2.146	1.104
	Double porosity model	3.074	3.267	2.94	5.24E−6	2.042	0.604
Standard deviation	Purely advective model	1.193	19.313	3.64	5.39E−6	0.828	0.457
	ADE model	0.791	1.891	0.94	2.30E−6	0.694	0.368
	Double porosity model	1.186	19.182	3.07	1.42E−6	0.811	0.301
$P_-=0.05$	Purely advective model	2.025	0.728	1.23	5.09E−6	1.063	0.813
	ADE model	1.954	0.370	1.12	4.69E−6	1.479	0.729
	Double porosity model	2.019	1.016	1.13	3.31E−6	1.225	0.354
$P_+=0.95$	Purely advective model	5.829	27.338	9.67	2.33E−5	3.696	2.231
	ADE model	4.253	4.779	4.05	1.17E−5	3.652	1.729
	Double porosity model	5.808	27.938	9.35	7.96E−6	3.546	1.273

One of the main features of the observed BTC is the pronounced tailing. In our numerical simulations the resulting slope is a consequence of two concurring factors: (1) the randomness of the hydraulic properties and (2) the choice of the transport model. We calculated the tail slope of each individual Monte Carlo BTC by plotting the latter in a semilog scale and then on the basis of least square regression of tail values. Fig. 10 reports the frequency distribution of the tail slope for all 100 simulations based on the geostatistical model HM2 and for the three different transport models investigated. Main slope statistics are reported, together with the slope of the tail of the experimental depth-integrated BTC. It is clear that the ensemble average and median slope of all three transport models tend to overestimate the experimental result, while only a few realizations provide a result that is close to (or smaller than) the observed one. From Fig. 10 it can also be observed that the ADE model provides the worst

representation (in statistical terms) of the observed tail slope in the experiment.

4.2. Multilevel breakthrough curves

We start by noting that the strongly heterogeneous distribution of geomaterials at the site favors the occurrence of preferential flow paths that heavily condition the transport process. Thus, as noted in Section 2.3, mass recovery at the pumping well is not uniformly distributed along the vertical, and this is likely due to the fact that the intermediate sampling levels (level 2 and 3, respectively) are associated with low-conductive flow paths within the system.

The conclusions presented in Section 4.1 regarding the effect of the choice of the conceptual model of aquifer
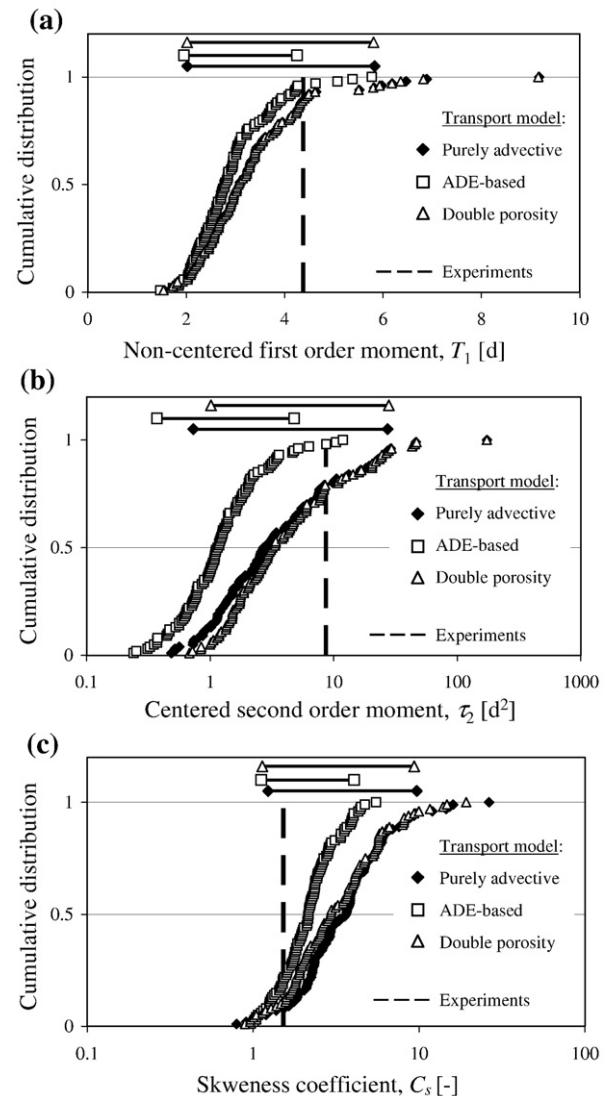

Fig. 8. Cumulative distributions of (a) T_1, (b) τ_2, and (c) C_s as obtained on the basis of numerical Monte Carlo iterations for the depth-averaged BTC and the three transport models tested. The experimental value observed is also reported together with the width of the interval including 90% of the realizations (i.e., the difference between the values associated with probabilities 0.05, and 0.95).
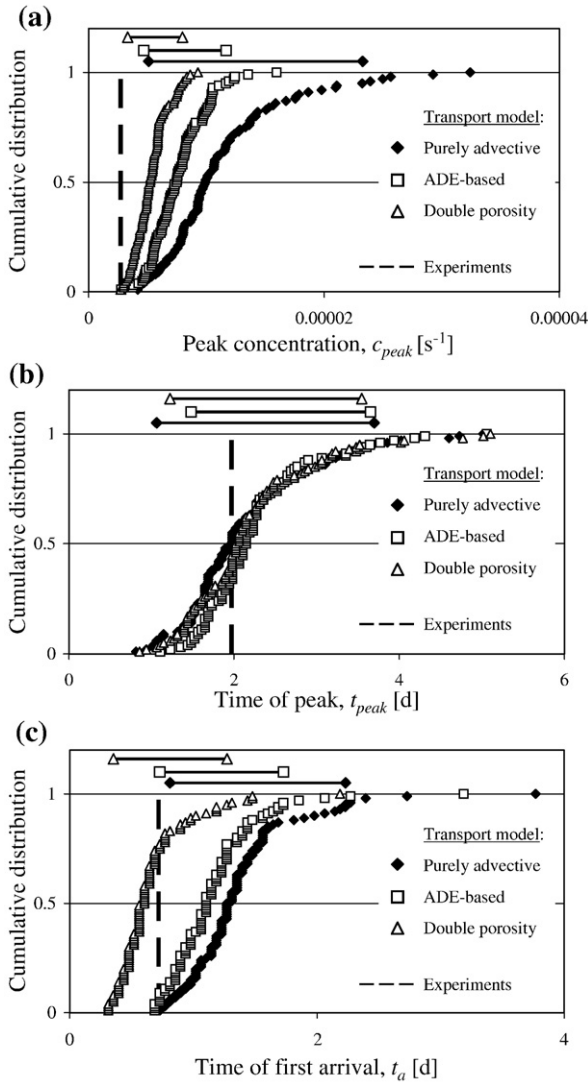
Fig. 9. Cumulative distributions of (a) c_{peak}, (b) t_{peak}, and (c) t_a as obtained on the basis of numerical Monte Carlo iterations for the depth-averaged BTC and the three transport models tested. The experimental value observed is also reported together with the width of the interval including 90% of the realizations (i.e., the difference between the values associated with probabilities 0.05, and 0.95).

Monte Carlo-based numerical BTCs are also presented in terms of consistently normalized concentrations.

While the models adopted provide a reasonable approximation for the BTCs corresponding to levels 1 and 4, the (ensemble) reproduction for levels 2 and 3 is quite poor. This is probably due to the type and quantity of measurements performed at the site for the characterization of the heterogeneous distribution of materials and associated attributes. While the data are sufficiently adequate to describe the most conducive paths between injection and recovery well, more refined measurements appear to be needed to characterize the less conductive regions. This is consistent with the structure of the system, where a main matrix of relatively high conductivity (identified with geomaterials belonging to cluster 1) can be found.

As a consequence, we note that the available information allows describing the vertically averaged features of
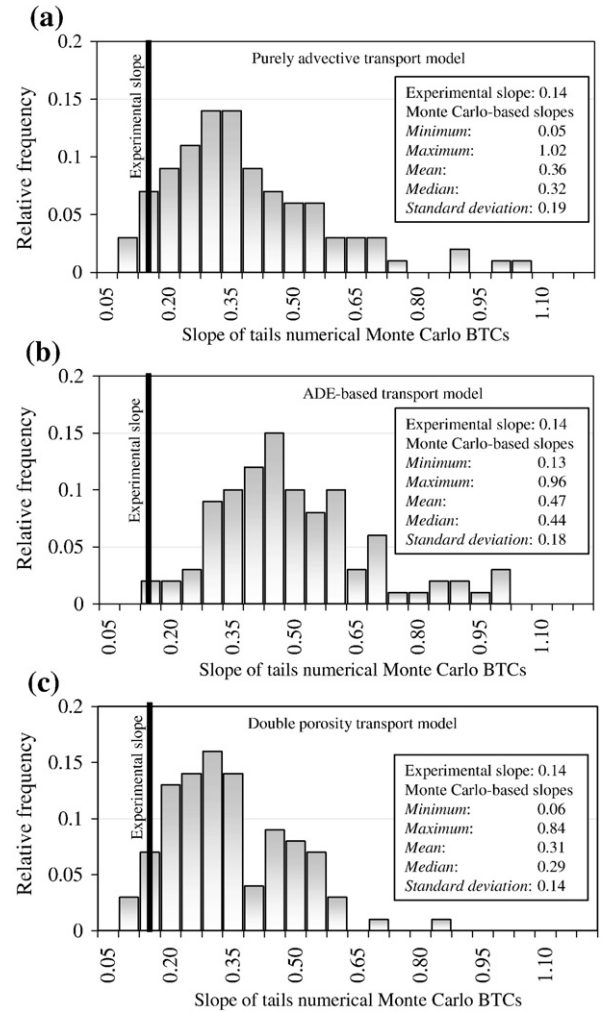

Fig. 10. Frequency distribution of the slope of the tails of the Monte Carlo-based depth-averaged BTCs (as calculated from a semilog representation of the BTCs) for all 100 simulations based on the geostatistical heterogeneity model HM2 when transport is depicted by means of (a) purely advective process, (b) an ADE and (c) a double porosity model. Main slope statistics are reported, together with the slope of the tail of the experimental depth-integrated BTC.
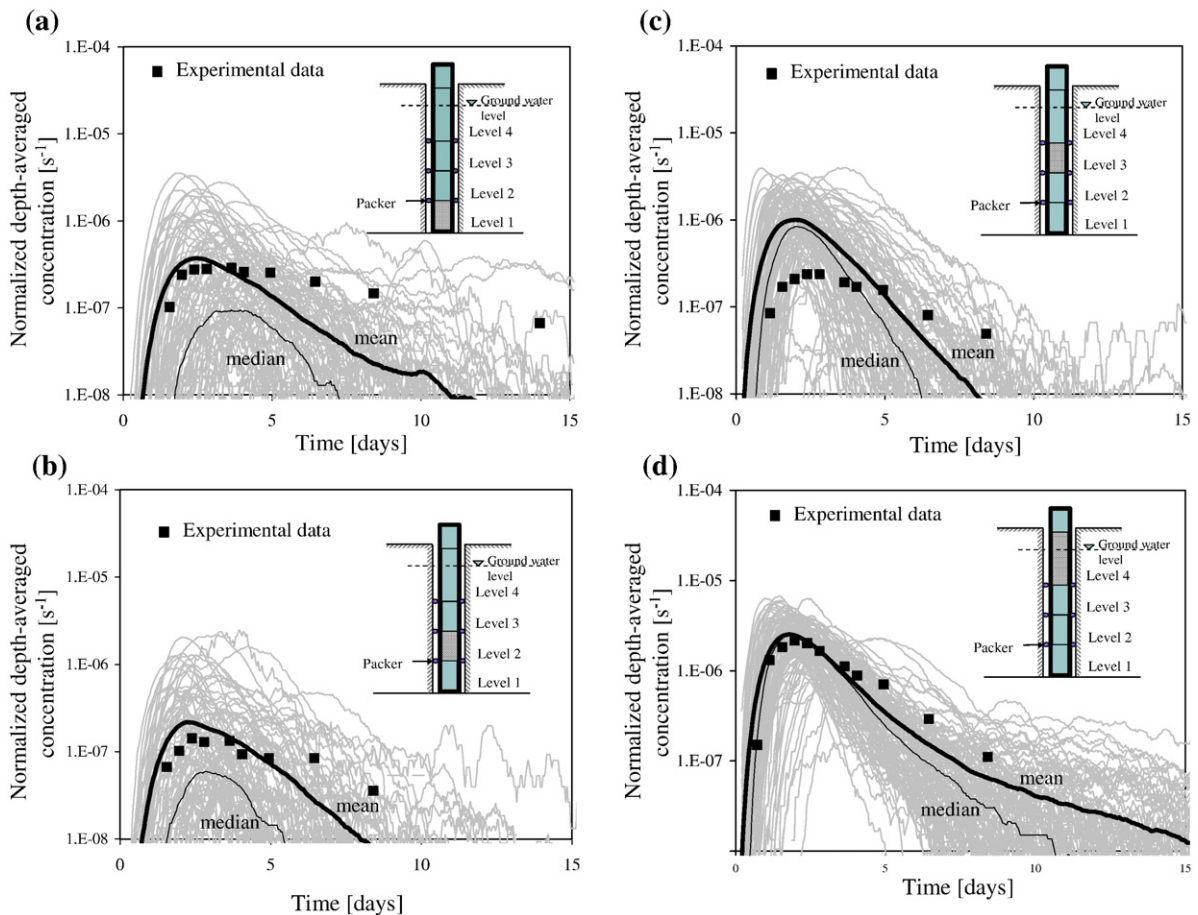
heterogeneity on the integrated BTC can be extended to the individual multilevel BTCs. Fig. 11 reports the field data corresponding to the BTCs recorded at levels 1 to 4, together with the probabilistic results obtained by 100 Monte Carlo simulations (including ensemble average and median BTCs) with the transport parameters adopted in Section 4.1. Here, for the purpose of illustration we only present the results corresponding to scenario HM2 and the double porosity model. The remaining transport models are conducive to similar plots in qualitative terms. The experimental BTC associated with sampling level j ($j = 1,..., 4$) is reported in terms of normalized concentrations, $c_j^{norm}(t)$ [s^{-1}], defined as

$$c_j^{norm}(t) = \frac{Q \cdot f_j \cdot c_j(t)}{m_0} \qquad (10)$$

Fig. 11. Multilevel normalized experimental BTC and ensemble mean and median Monte Carlo-based BTCs for geostatistical heterogeneity model HM2 when transport is depicted by means of a double porosity model for (a) level 1, (b) level 2, (c) level 3 and (d) level 4. Results associated with the complete set of Monte Carlo simulations are also reported.

transport at the site. At the same time, description of the most connected paths, on the basis of the available measurements, is sufficiently adequate to capture some of the three-dimensional transport features at the site, namely those associated with the levels where large mass recovery is observed.

5. Conclusions

Stochastic modeling of the non-Fickian behavior of breakthrough curves observed at the Lauswiesen forced-gradient tracer test experiment was performed to investigate the relative importance of the selection of (a) the conceptual model of the structural heterogeneity of the system and (b) the transport model adopted to represent basic processes involved in contaminant transport at the Darcy scale. Our work leads to the following major conclusions.

(1) An adequate description of heterogeneity, in this case by means of a doubly stochastic medium with random geological facies and hydraulic properties, is sufficient to capture the relevant features of the depth-averaged breakthrough curve, i.e., temporal moments and long tails.

(2) In this case, representation of the spatial distribution of porosity, in addition to hydraulic conductivity, is crucial to reproduce the early arrival of breakthrough curves. Nonetheless, the late-time behavior of breakthrough curves, in terms of the observed heavy tailing, is still mostly controlled by the spatial distribution of hydraulic conductivity and is not much influenced by the spatial fluctuations of porosity.

(3) Our simulations show that velocity fluctuations, which are likely enhanced by the forced-gradient conditions, largely dominate transport phenomena in the Lauswiesen site. Thus, formal inclusion of the local dispersive and subgrid mass-transfer processes in the transport model do not provide significant improvement.

(4) At least at the investigated scale, transport processes are primarily controlled by the spatial variability of hydraulic properties. This indicates that key aspects associated with reliable modeling of solute transport at the Lauswiesen site are not primarily included in the conceptual model of transport but in the interpretation and proper representation of the heterogeneity.

(5) Although the available description of heterogeneity can explain most of the integrated behavior of transport

(depth-averaged breakthrough curve), it does not ensure an adequate representation of the complete three-dimensional features of transport, since multi-level breakthrough curves associated with low conductive areas are not successfully reproduced (in a multirealization sense). Thus, our results indicate that an accurate description of the geometrical features of hydrofacies or of higher-order moments of the hydraulic properties is needed to completely describe the system. It is emphasized that caution must be taken in applying transport models which are based on integrated measurements, since use of vertically averaged information might not be sufficient to capture many of the important features required in a three-dimensional model.

Acknowledgements

References

Berkowitz, B., Cortis, A., Dentz, M., Scher, H., 2006. Modeling non-Fickian transport in geological formations as a continuous time random walk. Rev. Geophys. 44, RG2003. doi:10.1029/2005RG000178.

de Marsily, G., Delay, F., Gonçalvès, J., Renard, P., Teles, V., Violette, S., 2005. Dealing with spatial heterogeneity. Hydrogeology Journal 13, 161–183.

Deutsch, C.V., Journel, A.G., 1998. GSLIB Geostatistical Software Library and User's Guide, 2nd ed. Oxford Univ. Press, New York.

Fernandez-Garcia, D., Sanchez-Vila, X., Illangasekare, T.H., 2002. Convergent-flow tracer tests in heterogeneous media: combined experimental–numerical analysis for determination of equivalent transport parameters. J. Contam. Hydrol. 57 (1–2), 129–145.

Fernandez-Garcia, D., Illangasekare, T.H., Rajaram, H., 2005. Differences in the scale dependence of dispersivity and retardation factors estimated from forced-gradient and uniform flow tracer tests in three-dimensional physically and chemically heterogeneous porous media. Water Resour. Res. 41 (3). doi:10.1029/2004WR003523.

Gómez-Hernández, J.J., Journel, A., 1993. Joint simulation of multiGaussian random variables. Geostatistica Tróia '92, 1. Kluwer Academic Publishers, pp. 85–94.

Haggerty, R., Fleming, S.W., Meigs, L.C., McKenna, S.A., 2001. Tracer tests in fractured dolomite 2. Analysis of mass transfer in single-well injection-withdrawal tests. Water Resour. Res. 37 (5), 1129–1142.

Hassan, A.E., 2001. Water flow and solute mass flux in heterogeneous porous formations with spatially random porosity. J. Hydrology 242 (1–2), 1–25.

Harbaugh, A.W., Banta, E.R., Hill, M.C., McDonald, M.G., 2000. MODFLOW-2000, the U.S. Geological Survey modular ground-water model—User guide to modularization concepts and the Ground-Water Flow Process: U.S. Geological Survey Open-File Report 00-92, 121 p.

Juhasz, A., 2001. Field and numerical experiments to determine the hydraulic properties of gates applied at the funnel and gate system at the Beka site in Tuebingen. M.Sc. Thesis, University of Tübingen, Geological Institute.

LaBolle, E.M., Fogg, G.E., Tompson, A.F.B., 1996. Random-walk simulation of transport in heterogeneous porous media: local mass-conservation problem and implementation methods. Water Resour. Res. 32 (3), 583–593.

Martac, E., Ptak, T., 2003. Data sets for transport model calibration/validation, parameter upscaling studies and testing of stochastic transport models/theory. Report D16 of Project "Stochastic Analysis of Well-Head Protection and Risk Assessment—W-SAHaRA", EU contract EVK1-CT-1999-00041, Dipartimento Ingegneria Idraulica, Ambientale, Infrastrutture Viarie, Rilevamento, Politecnico di Milano, Milan, Italy.

McQueen, J., 1967. Some methods for classification and analysis of multivariate observations. 5th Berkeley Symposium on Mathematics, Statistics and Probability, vol. 1, pp. 281–298.

Ptak, T., Teutsch, G., 1994. A comparison of investigation methods for the prediction of flow and transport in highly heterogeneous formations. In: Dracos, T.H., Stauffer, F. (Eds.), Transport and Reactive Processes in Aquifers. Balkema, Rotterdam, pp. 157–164.

Ptak, T., Piepenbrink, M., Martac, E., 2004. Tracer tests for the investigation of heterogeneous porous media and stochastic modelling of flow and transport — a review of some recent developments. J. Hydrol. 294, 122–163.

Riva, M., Guadagnini, L., Guadagnini, A., Ptak, T., Martac, E., 2006. Probabilistic study of well capture zones distribution at the Lusweisen field site. J. Contam. Hydrol. 88, 92–118.

Sack-Kühner, B., 1996. Einrichtung des Naturmeßfeldes "Lauswiesen Tübingen", Erkundung der hydraulischen Eigenschaften, Charakterisierung der Untergrundheterogenität und Vergleich der Ergebnisse unterschiedlicher Erkundungsverfahren. Diplomarbeit im Fachbereich Geowissenschaften der Eberhard-Karls-Universität Tübingen, 96 Abb., 21 Tab., 147S.

Salamon, P., Fernàndez-Garcia, D., Gómez-Hernández, J.J., 2007. Modeling tracer transport at the MADE site: the importance of heterogeneity. Water Resour. Res. 43, W08404. doi:10.1029/2006WR005522.

Salamon, P., Fernàndez-Garcia, D., Gómez-Hernández, J.J., 2006. A review and numerical assessment of the random walk particle tracking method. J. Contam. Hydrol. 87 (3–4), 277–305.

Sanchez-Vila, X., Carrera, J., 1997. Directional effects on convergent flow tracer tests. Math. Geol. 29 (4), 551–569.

Sauty, J.P., 1980. An analysis of hydrodispersive transfer in aquifers. Water Resour. Res. 16 (1), 70–81.

Wen, X.H., Gómez-Hernández, J.J., 1996. The constant displacement scheme for tracking particles in heterogeneous aquifers. Ground Water 34 (1), 135–142.

Winter, C.L., Tartakovsky, D.M., Guadagnini, A., 2003. Moment differential equations for flow in highly heterogeneous porous media. Surv. Geophys. 24 (1), 81–106.